

Quantum Error Detection Without Using Ancilla Qubits

Nicolas J. Guerrero and David E. Weeks*

Air Force Institute of Technology

(Dated: April 26, 2022)

In this paper, we describe and experimentally demonstrate an error detection scheme that does not employ ancilla qubits or mid-circuit measurements. This is achieved by expanding the Hilbert space where a single logical qubit is encoded using several physical qubits. For example, one possible two qubit encoding identifies $|0\rangle_L = |01\rangle$ and $|1\rangle_L = |10\rangle$. If during the final measurement a $|11\rangle$ or $|00\rangle$ is observed an error is declared and the run is not included in subsequent analysis. We provide codewords for a simple bit-flip encoding, a way to encode the states, a way to implement logical U_3 and logical C_x gates, and a description of which errors can be detected. We then run Greenberger–Horne–Zeilinger circuits on the transmon based IBM quantum computers, with an input space of $N \in \{2, 3, 4, 5\}$ logical qubits and $Q \in \{1, 2, 3, 4, 5\}$ physical qubits per logical qubit. The results are compared relative to $Q = 1$ with and without error detection and we find a significant improvement for $Q \in \{2, 3, 4\}$.

I. INTRODUCTION

In an ideal world, physical qubits of quantum computers would be isolated from outside influence to permit useful and reliable quantum computation. Of course, it is well understood that such perfect isolation is likely an impossibility, and that there are many things interacting with quantum computers which prevent perfect qubits. These include, but are not limited to quantum vacuum fluctuations [1, 2], cosmic radiation [3–5], material defects [6–8], and many others.

The most promising idea to mitigate these errors is currently quantum error correction (QEC) and quantum error detection (QED). The first error correction code employed nine physical qubits per logical qubit and six ancilla qubits for syndrome extraction [9]. More efficient codes were soon produced such as codes on seven qubits [10] and five qubits [11], as well as other error correction schemes such as surface codes [12] and continuous QEC [13, 14]. These codes have been studied extensively through simulations [15–17] as well as more recently through experimentation [18–22].

In a similar manner, QED was first described using four physical qubits per logical qubit and two ancilla qubits for syndrome extraction [23]. Other types of detection process exist such as QED in surface codes [24] and hardware based sensors [25]. QED has been experimentally verified for small numbers of logical qubits [24, 26] and continues to be a useful companion to QEC. In this paper, we will introduce and experimentally verify a new type of quantum error detection which differs significantly from both QEC and QED. The experimental verification is conducted on the transmon based IBM quantum computers [27].

A. No ancilla error detection

No ancilla error detection (NAED) is a comparable process to both QEC and QED. In all three, Q physical qubits represent a single logical qubit with states $|0\rangle_L$ and $|1\rangle_L$. NAED differs from QEC and the standard QED in the rather obvious way that it does not use ancilla qubits. This has two benefits over previous schemes: the resources required are generally less than QEC and QED and mid-circuit measurements are not a requirement for NAED. The only measurements are made at the end of the circuit, thereby bypassing any noise that might otherwise be incurred by measuring ancilla qubits.

An implementation of NAED begins by considering a single logical qubit $|\psi\rangle_L = \alpha|0\rangle_L + \beta|1\rangle_L$ over Q physical qubits. Define the set $H^+ = \{\alpha|0\rangle_L + \beta|1\rangle_L : |\alpha|^2 + |\beta|^2 = 1\}$ and define the set $H^- = \mathcal{H}_Q - H^+$ where we have used \mathcal{H}_Q to be the Hilbert space over the Q physical qubits. The basic premise behind NAED is that a detectable error on any of the physical qubits will move a state $|\psi\rangle$ from H^+ to H^- . If the final state is measured and found to be in H^- , an error is declared. If not, then we measured something in H^+ and can identify that the logical qubit was measured in the $|0\rangle_L$ or $|1\rangle_L$ state. We stress that this scheme can produce false positives but no false negatives.

In this paper, we will describe a procedure to implement a simple NAED code. This includes the operators required to encode the initial states as well as methods to create logical gates out of the standard base set of U_3 and C_x gates. These logical gates are then used to produce logical Greenberger–Horne–Zeilinger (GHZ) states with differing amounts logical qubits and physical qubits per logical qubit. In general, constructing logical gates remains an active area of research for all error mitigation schemes [28–31].

The unencoded GHZ circuit can be thought of as generalized bell circuit and produces the state

* david.weeks@afit.edu

$$GHZ(N, 1) = \frac{|00\dots 0\rangle + |11\dots 1\rangle}{\sqrt{2}} \quad (1)$$

Here, there are N 0s and N 1s in each ket and the 1 in $GHZ(N, 1)$ represents the fact that there is no encoding with one physical qubit per logical qubit. We then run these circuits and compare the results with and without error detection.

II. BIT-FLIP ERROR DETECTION

The bit-flip encoding (based on classical Hamming Codes [32]) is the simplest NAED code. In general, a bit-flip encoding on Q physical qubits can be defined by a set $S \subseteq \{0, 1, \dots, Q-1\}$. We then define the two integers

$$x = \begin{cases} 0 & S = \emptyset \\ \sum_{i \in S} 2^i & \text{otherwise} \end{cases} \quad (2)$$

$$y = 2^Q - 1 - x \quad (3)$$

The code words are then defined as $|0\rangle_L = |x\rangle$ and $|1\rangle_L = |y\rangle$ where x and y are written in binary. From this, it is apparent that for Q physical qubits, there are 2^Q encodings that we might utilize. For example, a simple set of codewords for $Q = 3$ physical qubits is $|0\rangle_L = |001\rangle$ and $|1\rangle_L = |110\rangle$ as determined by the set $S = \{0\}$.

A word on the notation used throughout this paper: let σ_x be the standard 2×2 Pauli x matrix. We will use the notation σ_i to represent the $2^Q \times 2^Q$ matrix

$$\sigma_i = I_{2^i} \otimes \sigma_x \otimes I_{2^{Q-i-1}} \quad (4)$$

where I_n is the $n \times n$ identity matrix. For example, for $Q = 3$ we have

$$\sigma_0 = \sigma_x \otimes I_4 \quad (5)$$

$$\sigma_1 = I_2 \otimes \sigma_x \otimes I_2 \quad (6)$$

$$\sigma_2 = I_4 \otimes \sigma_x \quad (7)$$

Note that qubits are counted starting from 0 rather than 1.

For any two physical qubits in the circuit, the gate $C_x(i, j)$ is defined to be a controlled-not gate with control qubit i and target qubit j . Additionally, qubits other than i and j are assumed to be operated on by identity gates. The gate $C_x(i, j)$ represents a $2^n \times 2^n$ matrix,

rather than a 4×4 matrix, where n will be obvious from context. As an example, for $n = 3$ physical qubits

$$C_x(1, 2) = I_2 \otimes C_x \quad (8)$$

$$C_x(0, 2) = (I_2 \otimes SWAP)(C_x \otimes I_2)(I_2 \otimes SWAP) \quad (9)$$

$$C_x(1, 0) = (SWAP \cdot C_x \cdot SWAP) \otimes I_2 \quad (10)$$

Here, both C_x and $SWAP$ are the standard 4×4 controlled-not and swap gates respectively. Finally, when using product notation for matrix multiplication, we will use the convention

$$\prod_{n=1}^N A_n = A_N A_{N-1} \cdots A_2 A_1 \quad (11)$$

A. Encoding, Logical Gates, and Detectable Errors

In order use the bit-flip encoding, two things are required: a way to encode the initial $|0\rangle_L$ state and a method to construct logical gates that operate on $|0\rangle_L$ and $|1\rangle_L$. To encode $|0\rangle_L$ for a given set S (with Q physical qubits starting in the state $|00\dots 0\rangle$) we simply need to operate on each qubit q_i with a σ_x if $i \in S$. This can be written mathematically as

$$M_S = \prod_{i \in S} \sigma_i \quad (12)$$

where M_S is identified as the encoding matrix.

The construction of logical gates for the bit-flip encoding is slightly more complicated. By logical gates, we mean that a logical R gate (denoted $L_S(R)$) has the property $L_S(R)|\psi\rangle_L = |\phi\rangle_L$ when $R|\psi\rangle = |\phi\rangle$. Here, the subscript L denotes the logical version of non-encoded qubit states $|\psi\rangle$ and $|\phi\rangle$ and R is an arbitrary physical gate. For Q physical qubits and $S = \emptyset$ we have

$$L_{\emptyset}(U_3) = \left[\prod_{i=1}^{Q-1} C_x(0, Q-i) \right] U_3 \otimes I_{2^{Q-1}} \left[\prod_{i=1}^{Q-1} C_x(0, i) \right] \quad (13)$$

Note that this logical gate uses $2(Q-1)$ physical C_x gates. For a general set S we have

$$L_S(U_3) = \begin{cases} L_{\emptyset}(\sigma_x U_3 \sigma_x) & 0 \in S \\ L_{\emptyset}(U_3) & 0 \notin S \end{cases} \quad (14)$$

Finally, to define the logical C_x gate we must introduce some notation describing the physical qubits of

each logical qubit: let $\{r_0, r_1, \dots, r_{Q-1}\}$ be the Q physical qubits that correspond to the logical control qubit and let $\{p_0, p_1, \dots, p_{Q-1}\}$ be the Q physical qubits that correspond to the logical qubit being operated on. Then for an arbitrary S the logical C_x gate is given by

$$L_S(C_x) = \prod_{i=0}^{Q-1} C_x(r_i, p_i) (I_{2^Q} \otimes M_S) \quad (15)$$

Here, M_S is the encoding matrix defined in equation 12. Proofs of equations 14 and 15 are provided in the appendix.

An example of bit-flip encoding and the associated logical gates is given by encoding a bell state with $Q = 2$ and $S = \{1\}$. In this example $x = 2$ and $y = 1$ with $|0\rangle_L = |10\rangle$ and $|1\rangle_L = |01\rangle$. The circuit includes an encoding step, a logical Hadamard $L_{\{1\}}(H)$, and a logical controlled-not $L_{\{1\}}(C_X)$ as shown in FIG 1. The final state will be given by $|\psi\rangle = 1/\sqrt{2}(|00\rangle_L + |11\rangle_L) = 1/\sqrt{2}(|0101\rangle + |1010\rangle)$.

After measurement, there are 16 possibilities: 4 states in H^+ and 12 states in H^- . If we measure $|0101\rangle$ then we obtain $|00\rangle_L$. In a similar fashion $|1010\rangle$ yields $|11\rangle_L$, $|0110\rangle$ yields $|01\rangle_L$, and $|1001\rangle$ yields $|10\rangle_L$. If we measure any other of the 12 combinations of 0s and 1s, then we are in H^- and an error is declared.

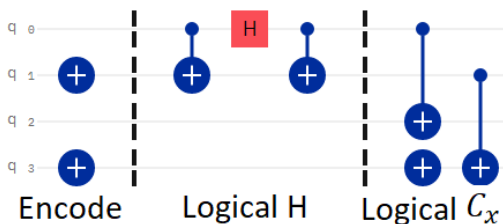


FIG. 1. This circuit encodes a bell state for $Q = 2$ physical qubits per logical qubit with codewords $|0\rangle_L = |01\rangle$ and $|1\rangle_L = |10\rangle$. The first set of gates to the left of the first barrier transforms $|0000\rangle$ to $|0101\rangle = |00\rangle_L$. The second set of gates is the logical Hadamard gate $L_{\{1\}}(H)$. The third set of gates is the logical C_x gate $L_{\{1\}}(C_X)$. At the end of this circuit, the qubits will be in the linear combination $|\psi\rangle = 1/\sqrt{2}(|00\rangle_L + |11\rangle_L) = 1/\sqrt{2}(|0101\rangle + |1010\rangle)$.

It is possible to describe the errors that we have a chance to detect while using the bit-flip code. If we model these errors by 2×2 unitary gates, then any error not of the form

$$P(\theta, \phi) = e^{i\phi} \begin{pmatrix} 1 & 0 \\ 0 & e^{i\theta} \end{pmatrix} \quad (16)$$

for real ϕ and $\theta \neq 2\pi k$, will force any state $|\psi\rangle \in H^+$ into some state $|\psi'\rangle \in H^-$. These detectable errors include σ_x , σ_y , and any other non-phase error that might occur.

III. AN APPLICATION OF THE BIT-FLIP ENCODING

The logical U_3 and C_x gates are used to construct $GHZ(N, Q)$ circuits where N is the number of logical qubits and Q is the number of physical qubits per logical qubit. Gates corresponding to this circuit are given by

$$GHZ(N, 1) = \left[\prod_{i=0}^{N-1} C_x(i, i+1) \right] (H \otimes I_{2^{N-1}}) \quad (17)$$

which uses $N - 1$ physical C_x gates and a single Hadamard gate. Note that this is not the only way to create the $GHZ(N, 1)$ state [33].

In order to turn the $GHZ(N, 1)$ circuit into the $GHZ(N, Q)$ circuit (using bit-flip encoding) we simply replace all physical gates in the $GHZ(N, 1)$ circuit with their logical equivalents from equations 14 and 15. Of course, we also have to decide which set S we will use for the encoding. In order to balance the number of 0s and 1s that make up $|0\rangle_L$ and $|1\rangle_L$, we will use $S = \{0, 1, \dots, \lceil Q/2 \rceil\}$. The last thing we need to do is slightly simplify the resulting circuit before implementation. For example, for the circuit $GHZ(2, 2)$ we have the circuit given in FIG 1, however the first C_x gate as well as the two σ_x gates on q_3 are redundant. Removing these gives us the circuit in FIG 2, and a similar simplification will be used for all experimental runs.

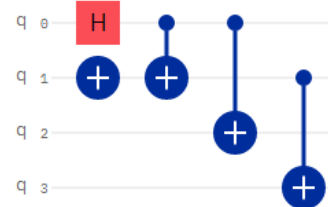


FIG. 2. The simplified $GHZ(2, 2)$ circuit. This circuit is identical to the circuit in FIG 1 except that the first C_x gate and bottom σ_x gates have been removed as redundant. This does not change the overall state $|\psi\rangle = 1/\sqrt{2}(|0101\rangle + |1010\rangle)$ that this circuit produces.

A. Experimental Design, Results, and Discussion

In order to measure how well our NAED works, we will employ a modified version of the total variation distance [34] between probability measure denoted $\tau(A, B)$ for finite probability distribution functions (PDFs) A and B . Define the similarity between two finite PDFs to be

$$\begin{aligned}
0 \leq \mu(A, B) &= 100(1 - \tau(A, B)) \\
&= 100 - 50 \sum_{i=1}^{|A|} |A_i - B_i| \leq 100 \quad (18)
\end{aligned}$$

The similarity is equal to 0 if two PDFs are completely dissimilar and 100 if they are identical. For our experiments we will use the IBMQ quantum computers and compare the experimentally determined PDF for the $GHZ(N, Q)$ circuit with theoretical expected PDF. For the simple $GHZ(N, Q)$ circuit, this theoretical PDF is easily computed and will always be an equally split between two states in the full \mathcal{H}_{NQ} circuit space.

All experiments were performed on the 27 qubit processor *ibmq_montreal* [27] with a quantum volume [35] of 128. For each $(N, Q) \in \{2, 3, 4, 5\} \times \{1, 2, 3, 4, 5\}$, the $GHZ(N, Q)$ circuit was submitted at optimization level 1 for 2^{13} shots. Two similarity measures are computed using equation 18. The first retains all of the experimental results and represents the full similarity measure of the encoded circuit, μ_{Full} . The second omits all experimental results for which an error is detected and is the NAED result, denoted μ_{NAED} . This process was repeated between 220 and 230 times for each circuit, and averaged to yield μ_{Full} and μ_{NAED} for each (N, Q) pair.

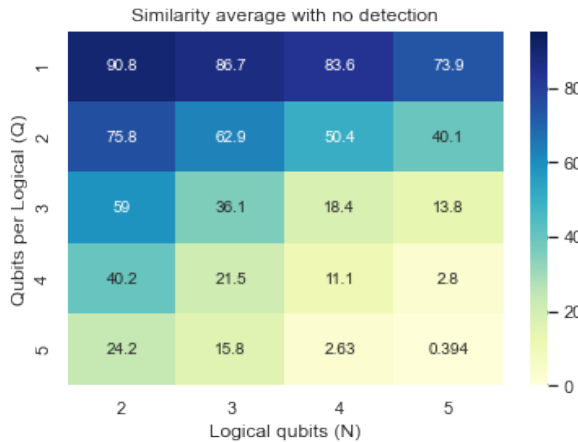


FIG. 3. The similarity measure μ_{Full} of the $GHZ(N, Q)$ circuits over the input space $(N, Q) \in \{2, 3, 4, 5\} \times \{1, 2, 3, 4, 5\}$. Not surprisingly, the best results occur at $GHZ(2, 1)$ with a similarity measure of 90.8. The similarity decreases as both N and Q increase, with the worst similarity of 0.4 for $N = Q = 5$.

Values of μ_{Full} are shown in FIG 3 where the best run overall is the $GHZ(2, 1)$ circuit with a similarity measure of 90.8. The similarity then decreases as both N and Q increase. Values of μ_{NAED} are shown in FIG 4 and

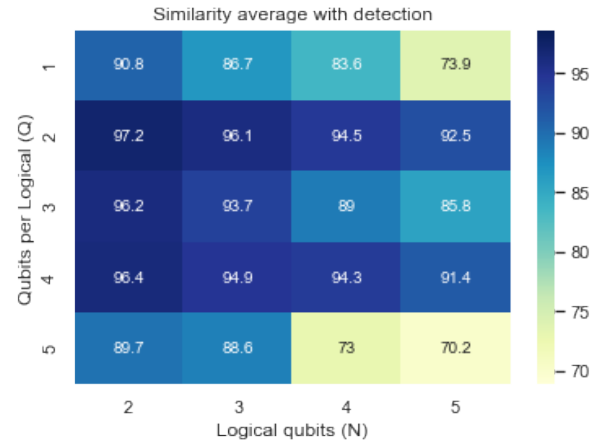


FIG. 4. The similarity measure μ_{NAED} of the $GHZ(N, Q)$ circuits over the input space $(N, Q) \in \{2, 3, 4, 5\} \times \{1, 2, 3, 4, 5\}$. The highest similarity is now 97.2 for $GHZ(2, 2)$ with the circuit from FIG 2. while the greatest increase in similarity from the unencoded circuit occurs between $GHZ(5, 1)$ and $GHZ(5, 2)$.

demonstrate that NAED is a viable option for improving quantum computation. As seen in FIG 4, values of μ_{NAED} for $GHZ(N, Q)$ where $2 \leq Q \leq 4$ are all greater than μ_{NAED} for the unencoded $GHZ(N, 1)$ circuit. It is not until $Q = 5$ that NAED produced lower values of μ_{NAED} than $Q = 1$ where no error detection is performed.

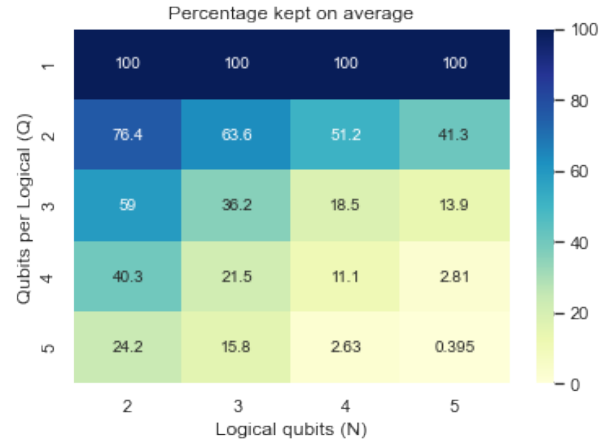


FIG. 5. The percentage of runs retained for each $GHZ(N, Q)$ circuit over the input space $(N, Q) \in \{2, 3, 4, 5\} \times \{1, 2, 3, 4, 5\}$ after error detection has been performed. For $Q = 1$, there are no runs removed. The next highest percentage is for the $GHZ(2, 2)$ circuit (given by FIG 2) at 76.4% kept. From here, the percentage retained decreases as both N and Q increase.

Also seen in FIG 4 is evidence that even values of Q outperform odd values of Q . For example, the similarity of $GHZ(N, 4)$ is greater than the similarity of $GHZ(N, 3)$ for all N . This behavior is caused by an asymmetry in the number of 0's and 1's that make up

the codewords for odd values of Q . Since superconducting qubits will naturally decohere towards the $|0\rangle$ state [36, 37], this leads to an asymmetry in measured states for odd Q .

A primary cost of NAED is the number of runs that are discarded when an error is declared. The total number of runs that are not included in the calculation of μ_{NAED} increases with N and Q as seen in FIG 5 where only a few percent of the runs are retained for larger N and Q . It is interesting to note the values of μ_{Full} in FIG 3 and percentage retained in FIG 5 approach each other in value as both N and Q increase. This observation is used to show that the ratio of false positives to the total number of measurements decreases as N and Q increase. To illustrate why this is the case, define the following

- T = the total number of measurements
- r_0 = the total number of $|00\dots 0\rangle_L$ measured
- r_1 = the total number of $|11\dots 1\rangle_L$ measured
- r_a = the total number of logical states other than $|00\dots 0\rangle_L$ or $|11\dots 1\rangle_L$ measured
- r_b = the total number of states which don't fall into any logical state measured

Here, r_b are errors that NAED would catch while r_a are errors that NAED would not catch. For example, with $N = 3$ and $Q = 2$ the state $|010110\rangle = |001\rangle_L$ is an invalid GHZ state but will not be caught by error detection. Also note that $T = r_0 + r_1 + r_a + r_b$. Then the percentage of measurements kept is given by

$$P_{Kept} = 1 - \frac{r_b}{T} \quad (19)$$

Without detection, μ_{Full} can be written as

$$\mu_{Full} = 1 - \frac{1}{2} \left(\left| \frac{1}{2} - \frac{r_0}{T} \right| + \left| \frac{1}{2} - \frac{r_1}{T} \right| + \frac{r_a}{T} + \frac{r_b}{T} \right) \quad (20)$$

The absolute values may be ignored since the chance that $\frac{r_0}{T} > \frac{1}{2}$ or $\frac{r_1}{T} > \frac{1}{2}$ is negligible for higher N and Q . Then equation 20 becomes

$$\begin{aligned} \mu_{Full} &= 1 - \frac{1}{2T}(T - r_0 - r_1 + r_a + r_b) \\ &= 1 - \frac{1}{2T}(T - r_0 - r_1 - r_a - r_b + 2r_a + 2r_b) \\ &= 1 - \frac{r_a}{T} - \frac{r_b}{T} = P_{Kept} - \frac{r_a}{T} \end{aligned} \quad (21)$$

As N and Q increase, the value of r_a/T in equation 21 goes to zero.

IV. CONCLUSION

These experiments have shown that NAED is a viable option for increasing the fidelity of quantum circuits. At its best, it was able to improve the similarity measure of a $GHZ(5, 1)$ circuit from $\mu_{Full} 73.9$ to $\mu_{NAED} 92.5$ using a $GHZ(5, 2)$ circuit. Additionally, we have shown that the ratio of false positives to the total number of measurements decreases as the number of logical qubits and the number of physical qubits per logical qubits increase. Current efforts are focused on expanding NAED to other encoding algorithms. As a final comment, NAED may provide higher fidelity quantum communication applications.

ACKNOWLEDGMENTS

The authors would like to thank the Air Force Research Laboratory for providing access to the IBMQ quantum computer as well as Dr. L. D. Merkle for many useful discussions. The views expressed are those of the authors, and do not reflect the official policy or position of IBM or the IBM Quantum team.

Appendix: Proofs of Logical Gates

In order to prove the validity of the logical gates described in equations 14-15, we will use the following four identities:

$$(I_2 \otimes \sigma_x)C_x = C_x(I_2 \otimes \sigma_x) \quad (A.1)$$

$$(\sigma_x \otimes I_2)C_x(\sigma_x \otimes I_2) = (I_2 \otimes \sigma_x)C_x \quad (A.2)$$

$$\alpha|0\rangle_L + \beta|1\rangle_L = M_S(\alpha|00\dots 0\rangle + \beta|11\dots 1\rangle) \quad (A.3)$$

where M_S is the encoding matrix given in equation 12. The first two of these equations are easily checked while the third equation follows from the definition of M_S . For the rest of these proofs, we will drop the S subscript and simply refer to the encoding matrix as M . After noting that $M = M^\dagger = M^{-1}$, this also gives us

$$M(\alpha|0\rangle_L + \beta|1\rangle_L) = \alpha|00\dots 0\rangle + \beta|11\dots 1\rangle \quad (A.4)$$

1. Logical U_3 gate

We will start with the $S = \emptyset$ case (with codewords $|0\rangle_L = |00\dots 0\rangle$ and $|1\rangle_L = |11\dots 1\rangle$) and from there prove the general case. To prove that $L_\emptyset(U_3)$ is a logical U_3

gate, we must show that if $U_3(\alpha|0\rangle + \beta|1\rangle) = \tau|0\rangle + \delta|1\rangle$ then $L_\emptyset(U_3)(\alpha|0\rangle_L + \beta|1\rangle_L) = \tau|0\rangle_L + \delta|1\rangle_L$. With the first part of $L_\emptyset(U_3)$ we have

$$\begin{aligned} |\psi_1\rangle &= \left[\prod_{i=1}^{Q-1} C_x(0, i) \right] (\alpha|0\rangle_L + \beta|1\rangle_L) \\ &= \alpha|00\dots 0\rangle + \beta|10\dots 0\rangle = (\alpha|0\rangle + \beta|1\rangle) \otimes |00\dots 0\rangle \quad (\text{A.5}) \end{aligned}$$

where the state $|00\dots 0\rangle$ in the resulting expression has $Q - 1$ zeros. Then applying the U_3 gate gives us

$$\begin{aligned} |\psi_2\rangle &= U_3 \otimes I_{2^{q-1}} |\psi_1\rangle = U_3 \otimes I_{2^{q-1}} (\alpha|0\rangle + \beta|1\rangle) \otimes |00\dots 0\rangle \\ &= (\tau|0\rangle + \delta|1\rangle) \otimes |00\dots 0\rangle \quad (\text{A.6}) \end{aligned}$$

The final part of $L_\emptyset(U_3)$ gives us

$$\begin{aligned} |\psi_3\rangle &= \left[\prod_{i=1}^{Q-1} C_x(0, Q - i) \right] |\psi_2\rangle \\ &= \left[\prod_{i=1}^{Q-1} C_x(0, Q - i) \right] (\tau|0\rangle + \delta|1\rangle) \otimes |00\dots 0\rangle \\ &= \tau|00\dots 0\rangle_L + \delta|11\dots 1\rangle_L = \tau|0\rangle_L + \delta|1\rangle_L \quad (\text{A.7}) \end{aligned}$$

as desired.

For the general case, if $0 \notin S$ then

$$L_S(U_3)(\alpha|0\rangle_L + \beta|1\rangle_L) = L_\emptyset(U_3)(\alpha|0\rangle_L + \beta|1\rangle_L)$$

$$= L_\emptyset(U_3)MM(\alpha|0\rangle_L + \beta|1\rangle_L) = L_\emptyset(U_3)M(\alpha|00\dots 0\rangle + \beta|11\dots 1\rangle) \quad (\text{A.8})$$

We also know that $[L_\emptyset(U_3), M] = \hat{0}$ since every C_x in $L_\emptyset(U_3)$ is controlled by q_0 , the physical U_3 gate in $L_\emptyset(U_3)$ acts on q_0 , and $0 \notin S$ which allows us to use equation A.1. Thus, equation A.8 becomes

$$\begin{aligned} &= L_\emptyset(U)M(\alpha|00\dots 0\rangle + \beta|11\dots 1\rangle) \\ &= ML_\emptyset(U)(\alpha|00\dots 0\rangle + \beta|11\dots 1\rangle) \\ &= M(\tau|00\dots 0\rangle + \delta|11\dots 1\rangle) = \tau|0\rangle_L + \delta|1\rangle_L \quad (\text{A.9}) \end{aligned}$$

For the case where $0 \in S$, let $M' = \sigma_1 M$. Then using the fact $\sigma_i = \sigma_i^{-1}$, we have

$$L_\emptyset(\sigma_x U_3 \sigma_x)M = \sigma_0 \sigma_0 L_\emptyset(\sigma_x U_3 \sigma_x) \sigma_0 M' \quad (\text{A.10})$$

Then using equation A.2 $2(Q - 1)$ times (one for each physical C_x in $L_\emptyset(\sigma_x U \sigma_x)$) and simplifying using equation A.1 we get

$$= \sigma_0 M' M' L_\emptyset(U_3) M' = ML_\emptyset(U_3) \quad (\text{A.11})$$

Using this relation we may now conclude

$$\begin{aligned} L_S(U_3)(\alpha|0\rangle_L + \beta|1\rangle_L) &= L_\emptyset(\sigma_x U \sigma_x)(\alpha|0\rangle_L + \beta|1\rangle_L) \\ &= L_\emptyset(\sigma_x U \sigma_x)MM(\alpha|0\rangle_L + \beta|1\rangle_L) = ML_\emptyset(U)(\alpha|00\dots 0\rangle + \beta|11\dots 1\rangle) \\ &= M(\tau|00\dots 0\rangle + \delta|11\dots 1\rangle) = \tau|0\rangle_L + \delta|1\rangle_L \quad (\text{A.12}) \end{aligned}$$

2. Logical C_x gate

In a similar manner to the previous proof, We will start with the $S = \emptyset$ case and from there prove the general case. To prove that $L_\emptyset(C_x)$ is a logical C_x gate, we must show that $L_\emptyset(C_x)(\alpha|00\rangle_L + \beta|01\rangle_L + \tau|10\rangle_L + \delta|11\rangle_L) = \alpha|00\rangle_L + \beta|01\rangle_L + \delta|10\rangle_L + \tau|11\rangle_L$. As in the main paper, let $\{r_0, r_1, \dots, r_{Q-1}\}$ be the Q physical qubits the make up the logical control qubit and let $\{p_0, p_1, \dots, p_{Q-1}\}$ be the Q physical qubits that make up the logical target bit. For ease of notation, the full ket corresponding to these $2Q$ physical qubits shall be written as $|r_0 r_1 \dots r_{Q-1}; p_0 p_1 \dots p_{Q-1}\rangle$, note the semi-colon used to distinguish between both sets of qubits. We then have

$$\begin{aligned} &C_x(r_0, p_0)(\alpha|00\rangle_L + \beta|01\rangle_L + \tau|10\rangle_L + \delta|11\rangle_L) \\ &= C_x(r_0, p_0)(\alpha|00\dots 0; 00\dots 0\rangle + \beta|00\dots 0; 11\dots 1\rangle \\ &\quad + \tau|11\dots 1; 00\dots 0\rangle + \delta|11\dots 1; 11\dots 1\rangle) \\ &= \alpha|00\dots 0; 00\dots 0\rangle + \beta|00\dots 0; 11\dots 1\rangle \\ &\quad + \tau|11\dots 1; 10\dots 0\rangle + \delta|11\dots 1; 01\dots 1\rangle \quad (\text{A.13}) \end{aligned}$$

Repeating this process for the other $Q - 1$ physical C_x gates in $L_\emptyset(C_x)$ gives us the desired result. To generalize to all S , note that by equations A.1 and A.2 we have

$$+ \delta|11\dots100\dots0\rangle + \tau|11\dots111\dots1\rangle) \quad (\text{A.15})$$

$$L_S(C_x) = L_\emptyset(C_x)(I_{2^Q} \otimes M) = (I_{2^Q} \otimes M)L_\emptyset(C_x)$$

$$= (M \otimes I_{2^Q})L_\emptyset(C_x)(M \otimes I_{2^Q})$$

$$= (M \otimes M)L_\emptyset(C_x)(M \otimes I_{2^Q}) = (M \otimes M)L_\emptyset(C_x)(M \otimes M) \quad (\text{A.14})$$

Using this equivalent definition for $L_S(C_x)$, we get

$$L_S(C_x)(\alpha|00\rangle_L + \beta|01\rangle_L + \delta|10\rangle_L + \tau|11\rangle_L)$$

$$= (M \otimes M)L_\emptyset(C_x)(M \otimes M)(\alpha|00\rangle_L + \beta|01\rangle_L + \delta|10\rangle_L + \tau|11\rangle_L)$$

$$= (M \otimes M)L_\emptyset(C_x)(\alpha|00\dots000\dots0\rangle + \beta|00\dots011\dots1\rangle)$$

by equation A.4. But this is precisely the relationship we just showed (the $S = \emptyset$ encoding). Thus, it simplifies to

$$= (M \otimes M)(\alpha|00\dots000\dots0\rangle + \beta|00\dots011\dots1\rangle)$$

$$+ \tau|11\dots100\dots0\rangle + \delta|11\dots111\dots1\rangle)$$

$$= \alpha|00\rangle_L + \beta|01\rangle_L + \tau|10\rangle_L + \delta|11\rangle_L \quad (\text{A.16})$$

as desired.

-
- [1] J. Q. You and F. Nori, Atomic physics and quantum optics using superconducting circuits, *Nature* **474**, 589 (2011).
- [2] C. Sabín, B. Peropadre, M. del Rey, and E. Martín-Martínez, Extracting past-future vacuum correlations using circuit qed, *Phys. Rev. Lett.* **109**, 033602 (2012).
- [3] A. D. Córcoles, J. M. Chow, J. M. Gambetta, C. Rigetti, J. R. Rozen, G. A. Keefe, M. B. Rothwell, M. B. Ketchen, and M. Steffen, Protecting superconducting qubits from radiation, *Applied Physics Letters* **99**, 181906 (2011).
- [4] A. P. Vepsäläinen, A. H. Karamlou, J. L. Orrell, A. S. Dogra, B. Loer, F. Vasconcelos, D. K. Kim, A. J. Melville, B. M. Niedzielski, J. L. Yoder, S. Gustavsson, J. A. Formaggio, B. A. VanDevender, and W. D. Oliver, Impact of ionizing radiation on superconducting qubit coherence, *Nature* **584**, 551 (2020).
- [5] C. D. Wilen, S. Abdullah, N. A. Kurinsky, C. Stanford, L. Cardani, G. D’Imperio, C. Tomei, L. Faoro, L. B. Ioffe, C. H. Liu, A. Opremcak, B. G. Christensen, J. L. DuBois, and R. McDermott, Correlated charge noise and relaxation errors in superconducting qubits, *Nature* **594**, 369 (2021).
- [6] S. S. Tannu and M. K. Qureshi, Not all qubits are created equal: A case for variability-aware policies for nisq-era quantum computers, in *Proceedings of the Twenty-Fourth International Conference on Architectural Support for Programming Languages and Operating Systems, ASPLOS ’19* (Association for Computing Machinery, New York, NY, USA, 2019) p. 987–999.
- [7] J. Lisenfeld, A. Bilmes, A. Megrant, R. Barends, J. Kelly, P. Klimov, G. Weiss, J. M. Martinis, and A. V. Ustinov, Electric field spectroscopy of material defects in transmon qubits, *npj Quantum Information* **5**, 105 (2019).
- [8] J. N. Eckstein and J. Levy, Materials issues for quantum computation, *MRS Bulletin* **38**, 783–789 (2013).
- [9] P. W. Shor, Scheme for reducing decoherence in quantum computer memory, *Phys. Rev. A* **52**, R2493 (1995).
- [10] A. M. Steane, Error correcting codes in quantum theory, *Phys. Rev. Lett.* **77**, 793 (1996).
- [11] D. P. DiVincenzo and P. W. Shor, Fault-tolerant error correction with efficient quantum codes, *Phys. Rev. Lett.* **77**, 3260 (1996).
- [12] A. Fowler, D. Wang, and L. Hollenberg, Surface code quantum error correction incorporating accurate error propagation, *Quantum information and computation* **11** (2010).
- [13] C. Ahn, A. C. Doherty, and A. J. Landahl, Continuous quantum error correction via quantum feedback control, *Phys. Rev. A* **65**, 042301 (2002).
- [14] G. Cardona, A. Sarlette, and P. Rouchon, Continuous-time quantum error correction with noise-assisted quantum feedback, *arXiv: Quantum Physics* (2019).
- [15] B. W. Reichardt, Fault-tolerant quantum error correction for steane’s seven-qubit color code with few or no extra qubits, *Quantum Science and Technology* **6**, 015007 (2020).
- [16] D. B. Trieu, *Large-scale simulations of error-prone quantum computation devices*, Ph.D. thesis (2009), cLASSICAL AND QUANTUM MECHANICS, GENERAL PHYSICS.
- [17] I. A. Simakov, I. S. Besedin, and A. V. Ustinov, Simulation of the five-qubit quantum error correction code on superconducting qubits (2021), *arXiv:2107.06491 [quant-ph]*.
- [18] L. Egan, D. M. Debroy, C. Noel, A. Risinger, D. Zhu, D. Biswas, M. Newman, M. Li, K. R. Brown, M. Cetina, and C. Monroe, Fault-tolerant operation of a quantum error-correction code (2021), *arXiv:2009.11482 [quant-*

- ph].
- [19] M. Gong, X. Yuan, S. Wang, Y. Wu, Y. Zhao, C. Zha, S. Li, Z. Zhang, Q. Zhao, Y. Liu, F. Liang, J. Lin, Y. Xu, H. Deng, H. Rong, H. Lu, S. C. Benjamin, C.-Z. Peng, X. Ma, Y.-A. Chen, X. Zhu, and J.-W. Pan, Experimental exploration of five-qubit quantum error correcting code with superconducting qubits, *National Science Review* 10.1093/nsr/nwab011 (2021), nwab011.
- [20] C. Ryan-Anderson, J. G. Bohnet, K. Lee, D. Gresh, A. Hankin, J. P. Gaebler, D. Francois, A. Chernoguzov, D. Lucchetti, N. C. Brown, T. M. Gatterman, S. K. Halit, K. Gilmore, J. Gerber, B. Neyenhuis, D. Hayes, and R. P. Stutz, Realization of real-time fault-tolerant quantum error correction (2021), arXiv:2107.07505 [quant-ph].
- [21] W. P. Livingston, M. S. Blok, E. Flurin, J. Dressel, A. N. Jordan, and I. Siddiqi, Experimental demonstration of continuous quantum error correction (2021), arXiv:2107.11398 [quant-ph].
- [22] Y. Ueno, M. Kondo, M. Tanaka, Y. Suzuki, and Y. Tabuchi, Qecool: On-line quantum error correction with a superconducting decoder for surface code (2021), arXiv:2103.14209 [quant-ph].
- [23] E. Knill, Quantum computing with realistically noisy devices, *Nature* **434**, 39 (2005).
- [24] C. K. Andersen, A. Remm, S. Lazar, S. Krinner, N. Lacroix, G. J. Norris, M. Gabureac, C. Eichler, and A. Wallraff, Repeated quantum error detection in a surface code, *Nature Physics* **16**, 875 (2020).
- [25] J. L. Orrell and B. Loer, Sensor-assisted fault mitigation in quantum computation, *Phys. Rev. Applied* **16**, 024025 (2021).
- [26] D. Ristè, S. Poletto, M.-Z. Huang, A. Bruno, V. Vesterinen, O.-P. Saira, and L. DiCarlo, Detecting bit-flip errors in a logical qubit using stabilizer measurements, *Nature Communications* **6**, 6983 (2015).
- [27] IBM Quantum, <https://quantum-computing.ibm.com/>, 2021.
- [28] J. F. Marques, B. M. Varbanov, M. S. Moreira, H. Ali, N. Muthusubramanian, C. Zachariadis, F. Battistel, M. Beekman, N. Haider, W. Vlothuizen, A. Bruno, B. M. Terhal, and L. DiCarlo, Logical-qubit operations in an error-detecting surface code (2021), arXiv:2102.13071 [quant-ph].
- [29] H. Chen, M. Vasmer, N. Breuckmann, and E. Grant, Machine learning logical gates for quantum error correction (2019).
- [30] F. Pastawski and B. Yoshida, Fault-tolerant logical gates in quantum error-correcting codes, *Phys. Rev. A* **91**, 012305 (2015).
- [31] L. Hu, Y. Ma, W. Cai, X. Mu, Y. Xu, W. Wang, Y. Wu, H. Wang, Y. P. Song, C.-L. Zou, S. M. Girvin, L.-M. Duan, and L. Sun, Quantum error correction and universal gate set operation on a binomial bosonic logical qubit, *Nature Physics* **15**, 503 (2019).
- [32] R. W. Hamming, Error detecting and error correcting codes, *The Bell System Technical Journal* **29**, 147 (1950).
- [33] D. Cruz, R. Fournier, F. Gremion, A. Jeannerot, K. Komagata, T. Tomic, J. Thiesbrummel, C. L. Chan, N. Macris, M. Dupertuis, and et al., Efficient quantum algorithms for ghz and w states, and implementation on the ibm quantum computer, *Advanced Quantum Technologies* **2**, 1900015 (2019).
- [34] L. Devroye, A. Mehrabian, and T. Reddad, The total variation distance between high-dimensional gaussians with the same mean (2018).
- [35] A. W. Cross, L. S. Bishop, S. Sheldon, P. D. Nation, and J. M. Gambetta, Validating quantum computers using randomized model circuits, *Phys. Rev. A* **100**, 032328 (2019).
- [36] J. J. Burnett, A. Bengtsson, M. Scigliuzzo, D. Niepce, M. Kudra, P. Delsing, and J. Bylander, Decoherence benchmarking of superconducting qubits, *npj Quantum Information* **5**, 54 (2019).
- [37] R. Youssef, Measuring and simulating t1 and t2 for qubits 10.2172/1656632 (2020).